NeRP: Implicit Neural Representation Learning with Prior Embedding for Sparsely Sampled Image Reconstruction

Image reconstruction is an inverse problem that solves for a computational image based on sampled sensor measurement. Sparsely sampled image reconstruction poses addition challenges due to limited measurements. In this work, we propose an implicit Neural Representation learning methodology with Prior embedding (NeRP) to reconstruct a computational image from sparsely sampled measurements. The method differs fundamentally from previous deep learning-based image reconstruction approaches in that NeRP exploits the internal information in an image prior, and the physics of the sparsely sampled measurements to produce a representation of the unknown subject. No large-scale data is required to train the NeRP except for a prior image and sparsely sampled measurements. In addition, we demonstrate that NeRP is a general methodology that generalizes to different imaging modalities such as CT and MRI. We also show that NeRP can robustly capture the subtle yet significant image changes required for assessing tumor progression.

I. Introduction

IMAGE reconstruction is conventionally formulated as an inverse problem, with the goal of obtaining the computational image of an unknown subject from measured sensor data. For example, projection data are measured for computed tomography imaging (CT) while frequency domain (k-space) data are sampled for magnetic resonance imaging (MRI). To reconstruct artifact-free images, dense sampling in measurement space is required to satisfy the Shannon-Nyquist theorem. However, in many practical applications it would be desirable to reconstruct images from sparsely sampled data. One important application is reducing radiation dose in CT imaging. Another application is accelerating MRI. The ill-posed nature of the sparse sampling image reconstruction problem poses a major challenge for algorithm development. Many approaches have been studied to solve this problem. One widely used approach is to exploit prior knowledge of the sparsity of the image in a transform domain, such as in compressed sensing, where total-variation, low-rank, and dictionary learning have been applied [1]-[7].

Unprecedented advances in deep learning driven by learning from large-scale data have achieved impressive progress in many fields, including computational image reconstruction. Many researchers have introduced deep learning models for medical imaging modalities such as CT and MRI [8], [9]. The key to these deep learning approaches is training convolutional neural networks (CNNs) to learn the mapping from raw measurement data to the reconstructed image by exploiting the large-scale training data. The network exploits the hidden transformation information embedded in the data through the data-driven training procedure. More advanced methods have improved the conventional deep learning reconstruction by leveraging prior knowledge from other aspects, such as generative adversarial model [10], [11] and geometry-integrated deep learning frameworks [12]-[15]. Previous works have demonstrated the effectiveness of explicitly incorporating physics and geometry priors of imaging system with deep learning [12], [15].

Although these works show the advantage of deep learning for medical image reconstruction, they have also exposed some limitations. For example, the acquisition of large-scale training data sets can be a bottleneck, the reconstructions may not be robust when deployed to unseen subjects, the reconstructions can be unstable with subtle yet significant structural changes such as tumor growth, and there can also be difficulties generalizing to different image modalities or anatomical sites [16]. To address these limitations, we propose a new insight for deep learning methodology for image reconstruction. We propose to learn the implicit Neural Representation of an image with Prior embedding (NeRP), instead of learning the reconstruction mapping itself. This is an essentially different perspective from previous deep learning-based reconstruction methods.

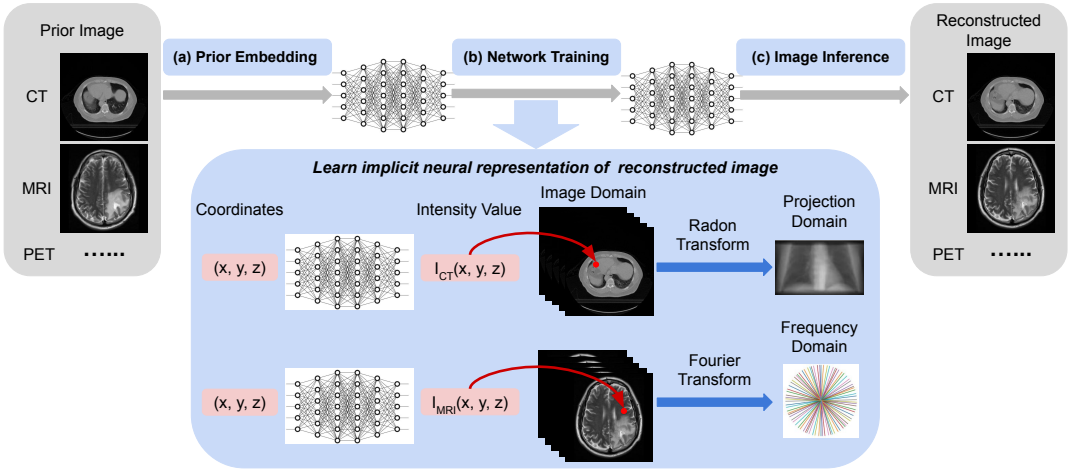

Fig. 1. Framework of implicit neural representation learning with prior embedding (NeRP) for image reconstruction.

Conventionally, a neural network is trained to learn the mapping from the sampled measurement data to reconstruct images based on a large-scale training database. The proposed NeRP model learns the network, i.e. multi-layer perceptron (MLP), to map the image spatial coordinates to the corresponding intensity values. The neural network learns the continuous implicit neural representation of the entire image by encoding the full image spatial field into the weights of MLP model [17], [18]. The image reconstruction problem is transformed into a network optimization problem. For sparse sampling, the measurements may not provide sufficient information to precisely reconstruct images of the unknown subject due to the ill-posed nature of the inverse problem. The proposed NeRP framework exploits prior knowledge from a previous image for the same subject. This is particularly applicable to clinical protocols where patients are scanned serially over time, such as monitoring tumor response to therapy. The implicit neural representation first embeds the internal information of the prior image into the weights of MLP. Note that NeRP requires no training data form external subjects except for the sparsely sampled measurements and a prior image of the subject.

The main contributions of this work are:

1) We present a novel deep learning methodology for sparsely sampled medical image reconstruction by learning the implicit neural representation of image with prior embedding (NeRP). Our method requires no training data from external subjects and can be easily generalized across different imaging modalities and contrasts, and different anatomical sites.

2) We propose a prior embedding method in implicit neural representation learning by encoding internal information of the prior image into network parameters as the initialization of network optimization, which enables sparsely sampled image reconstruction.

3) We present extensive experiments for both 2D and 3D image reconstruction with various imaging modalities, including CT and MRI, and demonstrate the effectiveness and generalizability of the proposed NeRP method. In particular, we show that our method is robust for capturing subtle yet significant structural changes such as those due to tumor progression.

II. Method

Fig. 1 illustrates the basic concept of the proposed implicit neural representation learning with prior embedding (NeRP) for image reconstruction. NeRP contains three modules to obtain the final reconstruction images. First, a prior image from earlier scan of the same subject is embedded as the implicit neural representation by encoding the entire spatial image field into the network's parameters. Specifically, the network is optimized to seek the continuous function that could precisely map the spatial coordinates to corresponding intensity values in the prior image. Next, using the prior-embedded network as the initialization, we aim to learn the neural representation of the target reconstruction image from the subsampled measurements of an unknown subject without any ground truth, as shown in Fig. 1(b). The differentiable forward model corresponding to the imaging system (e.g. Radon transform for CT imaging or Fourier transform for MRI imaging) is integrated to bridge between image space and sensor space. In this way, the network is optimized in the continuous function space of the network's parameters, with the constraints of the subsampled measurements from the unknown subject. Finally, the reconstructed image can be obtained by inferring the trained network across all the spatial coordinates in the image field.

A. Problem Formulation

To formulate the inverse problem for computational image reconstruction, the forward process of imaging system can be modeled as: $y = Ax + e$, where x is the image of the unknown subject while y is the sampled sensor measurements. Matrix A represents the forward model of the imaging system, and e is the acquisition noise.

Image reconstruction aims to recover the computational image x of the unknown subject, given the measurements y from sensors. In the sparsely sampled image reconstruction problem, the measurements y are undersampled in sensor space for either accelerated acquisition, as in MRI, or reduction of radiation, as in CT. The inverse problem for sparse sampling is ill-posed, and is typically formulated as an optimization problem with regularization: $x^* = \underset{x}{\operatorname{argmin}}\ \mathcal{E}(Ax, y) + \rho(x)$ where $\mathcal{E}(Ax, y)$ is the data term, which measures the errors between Ax and y, so as to guarantee the data consistency with the sensor measurements. Function $\mathcal{E}$ can be different distance metrics such as L1 or L2 norm. $\rho(x)$ is the regularizer term characterizing the generic image prior. The regularizer $\rho(x)$ can be determined in many different ways to capture various image characteristics. For example, total variation of the image enforces smoothness, while sparsity in a transform domain is used in compressed sensing.

B. Neural Representation for Image

In implicit neural representation learning, the image is represented by a neural network as a continuous function. The network $\mathcal{M}_\theta$ with parameters θ can be defined as: $\mathcal{M}_\theta: c \rightarrow v \ \ with \ \ c \in [0,1)^n,\ v \in \mathbb{R}$, where the input c is the normalized coordinate index in the image spatial field, and the output v is the corresponding intensity value in the image. The network function $\mathcal{M}_\theta$ maps coordinates to the image intensities, which actually encodes the internal information of entire image into the network parameters. Thus, network structure $\mathcal{M}_\theta$ with the parameters θ is also regarded as the neural representation for the image. Note that, theoretically, a random image in any modality or in any dimension $x \in \mathbb{R}^n$can be parameterized by the network using this method. Below we introduce the specific network structure used in our method.

1) Fourier Feature Embedding

Since Fourier features are shown to be effective for networks to learn high-frequency functions [20], we use a Fourier feature mapping γ to encode the input coordinates c before applying them to the coordinate-based network. Thus, the encoded coordinates are: $\gamma(c) = [\cos(2\pi Bc),\ \sin(2\pi Bc)]^T$, where matrix B represents the coefficients for Fourier feature transformation. Following [20], entries of matrix B are sampled

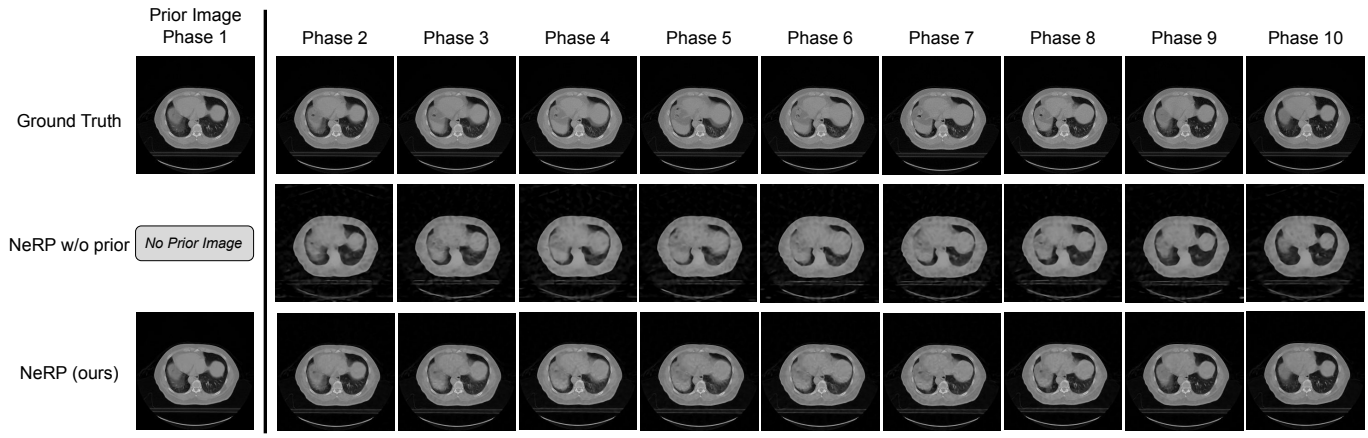

Fig. 2. Results of 2D CT image reconstruction for pancreas 4D CT data using 20 projections. The first row shows the ground truth cross-sectional 2D slices at the same location over 10 phases in the pancreas 4D CT, where each column demonstrates one phase respectively. The final row shows the reconstruction images at different phases respectively by using the proposed NeRP method, where the phase-1 image is used as the prior image for reconstructing the images in phase 2 ~ 10. For comparison, the second row shows the reconstruction results without using the prior embedding.

from Gaussian distribution $\mathcal{N}(0,\sigma^2)$, where σ is a hyperparameter characterizing the standard deviation of the prior distribution. After the Fourier feature embedding, the input to the network $\mathcal{M}_\theta$ is the encoded coordinates $\gamma(c)$.

2) Multi-Layer Perceptron Network

The network $\mathcal{M}_\theta$ is implemented by a deep fully-connected network or multi-layer perceptron (MLP). The coordinate-based MLP parameterizes the continuous function to represent the entire image. This function is defined by the network structure as well as the network parameters. In the next section, we will describe in detail how to obtain the network parameters through optimization. For the network structure, the model depth and width of MLP are hyper-parameters, characterizing the representative capability of the MLP model. Moreover, we use the periodic activation functions in our MLP model after each fully-connected layer, which are demonstrated to effectively represent fine details in signals [21].

C. NeRP for Sparsely Sampled Image Reconstruction

Next, we introduce how the proposed implicit neural representation learning with prior embedding (NeRP) is used to solve image reconstruction problem. The goal is to recover the image x of the target subject, given corresponding sparsely sampled measurements y and a prior image x^{pr}. Note that x^{pr} and x are different scans for the same subject, but at different time points. These capture the changing state of the subject such as tumor progression for monitoring therapy response.

1) Prior Embedding

In the first step, we embed the prior image x^{pr} into the network. We use the coordinate-based MLP $\mathcal{M}_\phi$ introduced in Sec.III.B to map the spatial coordinates to corresponding intensity values in prior image x^{pr}. That is, $\mathcal{M}_\phi: c_i \rightarrow x_i^{pr}$, where i denotes the coordinate index in image spatial field. Given all the coordinate-intensity pairs in prior image $\{c_i, x_i^{pr}\}_{i=1}^N$ with a total of N pixels in the image, the randomly-initialized MLP is optimized based on the objective:

$$\phi^* = \underset{\phi}{\operatorname{argmin}} \frac{1}{N}\sum_{i=1}^{N}\left\|\mathcal{M}_\phi(c_i) - x_i^{pr}\right\|_2^2 \qquad (1)$$

After optimization, the internal information of prior image x^{pr} is encoded into the MLP network $\mathcal{M}_{\phi^*}$ with the corresponding network parameters ϕ^*. For clarity, we use $\mathcal{M}^{pr}$ to denote the prior-embedded MLP network, i.e. $x^{pr} = \mathcal{M}_{\phi^*} = \mathcal{M}^{pr}$.

2) Network Training

Given the prior-embedded MLP $\mathcal{M}^{pr}$ and measurements y, we train the network to learn the neural representation of the target image. Based on the formulation in Eq. (2), the unknown target image x is parametrized by a coordinate-based MLP $\mathcal{M}_\theta$ with parameters θ. Thus, the data term is defined as $\min_x \mathcal{E}(Ax, y) = \min_\theta \mathcal{E}(A\mathcal{M}_\theta, y)$, where the optimization in image space is transformed to the optimization in the space of MLP's parameters. Furthermore, the regularizer $\rho(x)$ is replaced by the implicit image priors from network parametrization, including the internal information from prior image embedded in $\mathcal{M}^{pr}$ as well as the low-level image statistics prior captured by network structure itself $\mathcal{M}_\theta$ [24]. Thus, the optimization objective in Eq. (2) can be formulated as follows:

$$\theta^* = \underset{\theta}{\operatorname{argmin}}\ \mathcal{E}(A\mathcal{M}_\theta, y; \mathcal{M}^{pr}), \quad x^* = \mathcal{M}_{\theta^*} \qquad (2)$$

The network $\mathcal{M}_\theta$ is trained by minimizing the L2-norm loss, which is initialized by the prior-embedded network $\mathcal{M}^{pr}$. Note that forward model A is adapted to the corresponding imaging system, such as Radon transform for CT imaging and Fourier transform for MRI imaging. The operation A is differentiable, which enables training the network $\mathcal{M}_\theta$ in an end-to-end fashion.

3) Image Inference

Finally, after the network is well trained, the reconstruction image can be generated by inferring the trained network across all the spatial coordinates in the image field. That is: $x^*: \{c_i,\ \mathcal{M}_{\theta^*}(c_i)\}_{i=1}^N$, where i denotes the coordinate index in image spatial field. This is denoted in short as $x^* = \mathcal{M}_{\theta^*}$ in Eqs. (6) and (7). Filling the intensity values at all the coordinates in image grid constitutes the final reconstruction image x^*.

TABLE I
RESULTS OF 3D CT IMAGE RECONSTRUCTION
USING 5 / 10 / 20 PROJECTIONS ON DIFFERENT ANATOMICAL SITES

Methods	Pancreas CT	HeadNeck CT	Lung CT
Projections = 10			
FBP	17.95 / 0.461	23.05 / 0.653	21.49 / 0.597
GRFF [20]	28.07 / 0.855	29.38 / 0.864	27.80 / 0.835
NeRP w/o prior	28.88 / 0.850	30.40 / 0.858	30.98 / 0.880
NeRP (ours)	**37.66 / 0.981**	**36.92 / 0.976**	**32.73 / 0.941**
Projections = 20			
FBP	18.23 / 0.610	23.42 / 0.750	21.74 / 0.717
GRFF [20]	29.27 / 0.893	32.56 / 0.931	32.75 / 0.935
NeRP w/o prior	32.41 / 0.927	32.59 / 0.920	32.86 / 0.929
NeRP (ours)	**39.06 / 0.986**	**38.81 / 0.985**	**36.52 / 0.972**
Projections = 30			
FBP	18.31 / 0.650	23.54 / 0.773	21.83 / 0.7443
GRFF [20]	31.53 / 0.932	32.34 / 0.927	33.13 / 0.942
NeRP w/o prior	33.88 / 0.953	33.53 / 0.942	33.97 / 0.951
NeRP (ours)	**39.65 / 0.987**	**39.50 / 0.987**	**37.66 / 0.980**

Evaluation metric: PSNR / SSIM values are reported.
PSNR (dB), peak signal noise ratio; SSIM, structural similarity.

TABLE II
RESULTS OF 3D MRI IMAGE RECONSTRUCTION
USING 30 / 40 / 50 RADIAL SPOKES FOR DIFFERENT IMAGE CONTRASTS

Methods	T1	T1c	T2	FLAIR
Spokes = 30				
Adjoint NUFFT	20.91 / 0.63	21.68 / 0.63	19.55 / 0.57	19.77 / 0.58
GRFF [20]	27.98 / 0.90	27.67 / 0.88	25.66 / 0.85	25.98 / 0.86
NeRP w/o prior	27.49 / 0.85	27.82 / 0.87	25.91 / 0.85	26.87 / 0.88
NeRP (ours)	**28.43 / 0.90**	**29.06 / 0.92**	**26.86 / 0.90**	**27.52 / 0.90**
Spokes = 40				
Adjoint NUFFT	21.30 / 0.66	22.05 / 0.67	20.17 / 0.62	20.23 / 0.61
GRFF [20]	28.18 / 0.90	28.11 / 0.89	25.67 / 0.85	25.99 / 0.86
NeRP w/o prior	29.70 / 0.92	29.29 / 0.91	27.59 / 0.91	27.54 / 0.90
NeRP (ours)	**31.75 / 0.96**	**30.53 / 0.94**	**28.73 / 0.93**	**29.07 / 0.93**
Spokes = 50				
Adjoint NUFFT	21.40 / 0.68	22.26 / 0.69	20.42 / 0.64	20.49 / 0.64
GRFF [20]	28.50 / 0.91	27.59 / 0.88	25.23 / 0.85	25.90 / 0.87
NeRP w/o prior	30.65 / 0.94	29.26 / 0.91	28.40 / 0.92	27.68 / 0.90
NeRP (ours)	**32.55 / 0.96**	**31.37 / 0.95**	**30.13 / 0.95**	**30.02 / 0.94**

Evaluation metric: PSNR / SSIM values are reported.
PSNR (dB), peak signal noise ratio; SSIM, structural similarity.

III. EXPERIMENTS AND RESULTS

To evaluate the proposed NeRP method, we conducted experiments for 2D/3D CT and MRI image reconstruction with sparsely sampling. For CT image reconstruction we assume 20 projections equally distributed across a semi-circle. We compute parallel-beam projections for 2D CT and cone-beam projections for 3D CT. For MRI image reconstruction, 40 radial spokes are sampled in k-space with golden angle as the angular interval. Beyond sparsely-sampled measurements data, a prior image from an earlier scan is also given. Since the prior image and reconstruction image are of the same patient at different time points, the prior image can provide useful information about the patient's anatomic structure while still allowing crucial structural and functional differences such as tumor or lesion changes. We will show the experimental results applying NeRP for 2D/3D CT and MRI image reconstruction with various image contrasts and at various anatomical sites. The experiments datasets contain: (1) a pancreas 4D CT with 10 phases (phase 1 as the prior image); (2) two clinical patient cases including a head and neck CT case and a lung CT case, where each case has two longitudinal 3D CT images scanned for the same patient during radiation therapy (earlier CT as the prior image); (3) brain tumor regression MRI dataset: for each patient with primary newly diagnosed glioblastoma, there are two MRI exams within 90 days following chemo-radiation therapy completion and at tumor progression (set the first MRI exam as the prior image).

A. Experiments on CT Image Reconstruction

In Fig. 2, we show the 2D CT reconstruction results for phase 2 to phase 10 using the proposed NeRP algorithm by using phase 1 as prior image. The reconstructed images can precisely capture the continuous changes with fine detail over different phases, although the same prior image is used and only sparse projections are sampled for reconstructing the target image in each phase. For comparison, we conducted experiments to show the results of other reconstruction methods including filtered back projection (FBP) and Gaussian random Fourier feature (GRFF) [20]. Going beyond 4D CT data, we also evaluated the clinical radiation therapy patient data with both head and neck CT and lung CT. The quantitative results for 3D CT reconstruction evaluated by PSNR and SSIM metrics are reported in Table I on different anatomic sites with all comparison methods.

B. Experiments on MRI Image Reconstruction

We conducted experiments to evaluate the proposed method for MRI image reconstruction. Appendix Fig. S1 demonstrates 2D MRI reconstruction results for multi-contrast MR images. We can see the reconstructed images from sparsely subsampled k-space data can accurately capture the fine detailed structures especially in the tumor region, which differs from that in the prior image. Quantitative results of 3D MRI image reconstruction evaluated by PSNR and SSIM metrics are reported in Table II for different image contrasts including T1, T1c, T2 and FLAIR. The reconstruction results indicate that our method is able to reconstruct the precise changes in brain tumor region even with sparsely sampled k-space data, which is crucial for clinical diagnosis and cancer treatment.

IV. CONCLUSION

In this work, we propose a new deep learning-based medical image reconstruction methodology by learning implicit neural representations with prior embedding (NeRP), which efficiently incorporates the prior knowledge and learns to reconstruct the target image through implicit neural representations. Through the experiments for 2D/3D MRI and CT image reconstruction, we show that the proposed NeRP algorithm is able to provide high-quality reconstruction images even with sparsely sampled measurements data. The NeRP approach possesses a number of unique advantages: (1) requires no training data from external subjects for developing networks; (2) accurate reconstruction of small and detailed changes such as anatomic structure or tumor progression; (3) broad applicability to different body sites, different imaging modalities and different patients.

REFERENCES

[1] M. Lustig, D. Donoho and J.M. Pauly, "Sparse MRI: The application of compressed sensing for rapid MR imaging," *Magnetic Resonance in Medicine: An Official Journal of the International Society for Magnetic Resonance in Medicine*, *58*(6), pp.1182-1195, 2007.

[2] M. Lustig, D. L. Donoho, J. M. Santoss, and Pauly, J. M, "Compressed sensing MRI," *IEEE signal processing magazine*, *25*(2), 72-82, 2008.

[3] H. Yu and G. Wang, "Compressed sensing based interior tomography," *Phys. Med. Biol.* 54, 2791-2805, 2009.

[4] G. H. Chen, J. Tang and S. Leng, "Prior image constrained compressed sensing (PICCS): a method to accurately reconstruct dynamic CT images from highly undersampled projection data sets," *Med. Phys*. 35, 660-663, 2008.

[5] K. Choi *et al.,* "Compressed sensing based cone-beam computed tomography reconstruction with a first-order method," *Med. Phys*. 37, 5113-5125, 2010.

[6] E. Y. Sidky and X. Pan, "Image reconstruction in circular cone-beam computed tomography by constrained, total-variation minimization," *Phys. Med. Biol*. 53, 4777-4807, 2008.

[7] S. Ravishankar and Y. Bresler, "MR image reconstruction from highly undersampled k-space data by dictionary learning," *IEEE transactions on medical imaging*, *30*(5), pp.1028-1041, 2010.

[8] B. Zhu, J. Z. Liu, S. F. Cauley, B. R. Rosen, and M. S. Rosen, "Image reconstruction by domain-transform manifold learning," *Nature*, 555**,** 487-492, 2018.

[9] L. Shen, W. Zhao, and L. Xing, "Patient-specific reconstruction of volumetric computed tomography images from a single projection view via deep learning," *Nature Biomedical Engineering*, 3(11)**,** 880-888, 2019.

[10] M. Mardani *et al.,* "Deep generative adversarial neural networks for compressive sensing MRI," In *IEEE Transactions on Medical Imaging (TMI)*, 38(1), 167-179, 2018.

[11] X. Ying *et al.,* "X2CT-GAN: reconstructing CT from biplanar X-rays with generative adversarial networks," In *Proceedings of the IEEE Conference on Computer Vision and Pattern Recognition (CVPR)*, 10619-10628, 2019.

[12] L. Shen, W. Zhao, D. Capaldi, J. Pauly, and L. Xing, "Geometry-informed deep learning framework for ultra-sparse computed tomography (CT) imaging," In *Neural Information Processing Systems (NeurIPS) Deep Learning and Inverse Problems Workshop,* 2020.

[13] W.A. Lin, H. Liao, C. Peng, X. Sun, J. Zhang, J. Luo, R. Chellappa and S.K. Zhou. "Dudonet: Dual domain network for ct metal artifact reduction," In *Proceedings of the IEEE/CVF Conference on Computer Vision and Pattern Recognition*, pp. 10512-10521, 2019.

[14] T. Würfl, M. Hoffmann, V. Christlein, K. Breininger, Y. Huang, M. Unberath and A.K. Maier. "Deep learning computed tomography: Learning projection-domain weights from image domain in limited angle problems," *IEEE transactions on medical imaging*, *37*(6), pp.1454-1463, 2018.

[15] L. Shen, L. Yu, W. Zhao, J. Pauly, and L. Xing, "Novel-view x-ray projection synthesis through geometry-integrated deep learning," In *Medical Image Analysis, under review,* 2020.

[16] V. Antun, F. Renna, C. Poon, B. Adcock, and A. C. Hansen, "On instabilities of deep learning in image reconstruction and the potential costs of AI," *Proceedings of the National Academy of Sciences*, 117(48), 30088-30095, 2020.

[17] S. A. Eslami, *et al.,* "Neural scene representation and rendering," *Science*, 360(6394), pp. 1204-1210, 2018.

[18] V. Sitzmann, M. Zollhöfer, and G. Wetzstein. "Scene representation networks: Continuous 3d-structure-aware neural scene representations," In *Advances in Neural Information Processing Systems*, pp. 1121-1132, 2019.

[19] B. Mildenhall, P.P. Srinivasan, M. Tancik, J.T. Barron, R. Ramamoorthi and R. Ng, "Nerf: Representing scenes as neural radiance fields for view synthesis," In *European Conference on Computer Vision*, pp. 405-421, 2020.

[20] M. Tancik *et al.,* "Fourier features let networks learn high frequency functions in low dimensional domains," *Advances in Neural Information Processing Systems*, 2020.

[21] V. Sitzmann, J. Martel, A. Bergman, D. Lindell, and G. Wetzstein, "Implicit neural representations with periodic activation functions," *Advances in Neural Information Processing Systems*, 33, 2020.

[22] R. Martin-Brualla, N. Radwan, M.S. Sajjadi, J.T. Barron, A. Dosovitskiy and D. Duckworth, "Nerf in the wild: Neural radiance fields for unconstrained photo collections," In *Proceedings of the IEEE Conference on Computer Vision and Pattern Recognition (CVPR)*, 2021.

[23] Y. Sun, J. Liu, M. Xie, B. Wohlberg and U.S. Kamilov, "CoIL: Coordinate-based Internal Learning for Imaging Inverse Problems," *arXiv preprint arXiv:2102.05181*, 2021.

[24] D. Ulyanov, A. Vedaldi and V. Lempitsky, "Deep image prior," In *Proceedings of the IEEE conference on computer vision and pattern recognition*, pp. 9446-9454, 2018.

[25] Y. Gandelsman, A. Shocher and M. Irani, "'Double-DIP': Unsupervised Image Decomposition via Coupled Deep-Image-Priors," In *Proceedings of the IEEE/CVF Conference on Computer Vision and Pattern Recognition*, pp. 11026-11035, 2019.

[26] A. Paszke et al., "Automatic differentiation in PyTorch," in Proc. NIPS Autodiff Workshop, 2017.

[27] J. Adler, H. Kohr, O. Oktem, "Operator Discretization Library (ODL)," 2017.

[28] M. J. Muckley, R. Stern, T. Murrell and F. Knoll, "TorchKbNufft: A High-Level, Hardware-Agnostic Non-Uniform Fast Fourier Transform," *ISMRM Workshop on Data Sampling and Image Reconstruction*, 2020.

[29] KM. Schmainda and M. Prah, "Data from Brain-Tumor-Progression," *The Cancer Imaging Archive*, 2018. [Online] Available: http://doi.org/10.7937/K9/TCIA.2018.15quzvnb

[30] K. Clark *et al.,* "The Cancer Imaging Archive (TCIA): maintaining and operating a public information repository," *Journal of Digital Imaging*, 26(6), pp 1045-1057, 2013.

[31] L. Xing**,** M. L. Giger, and J. K. Min, "Artificial Intelligence in Medicine: Technical Basis and Clinical Applications", Academic Press, London, UK, 2020.

Appendix

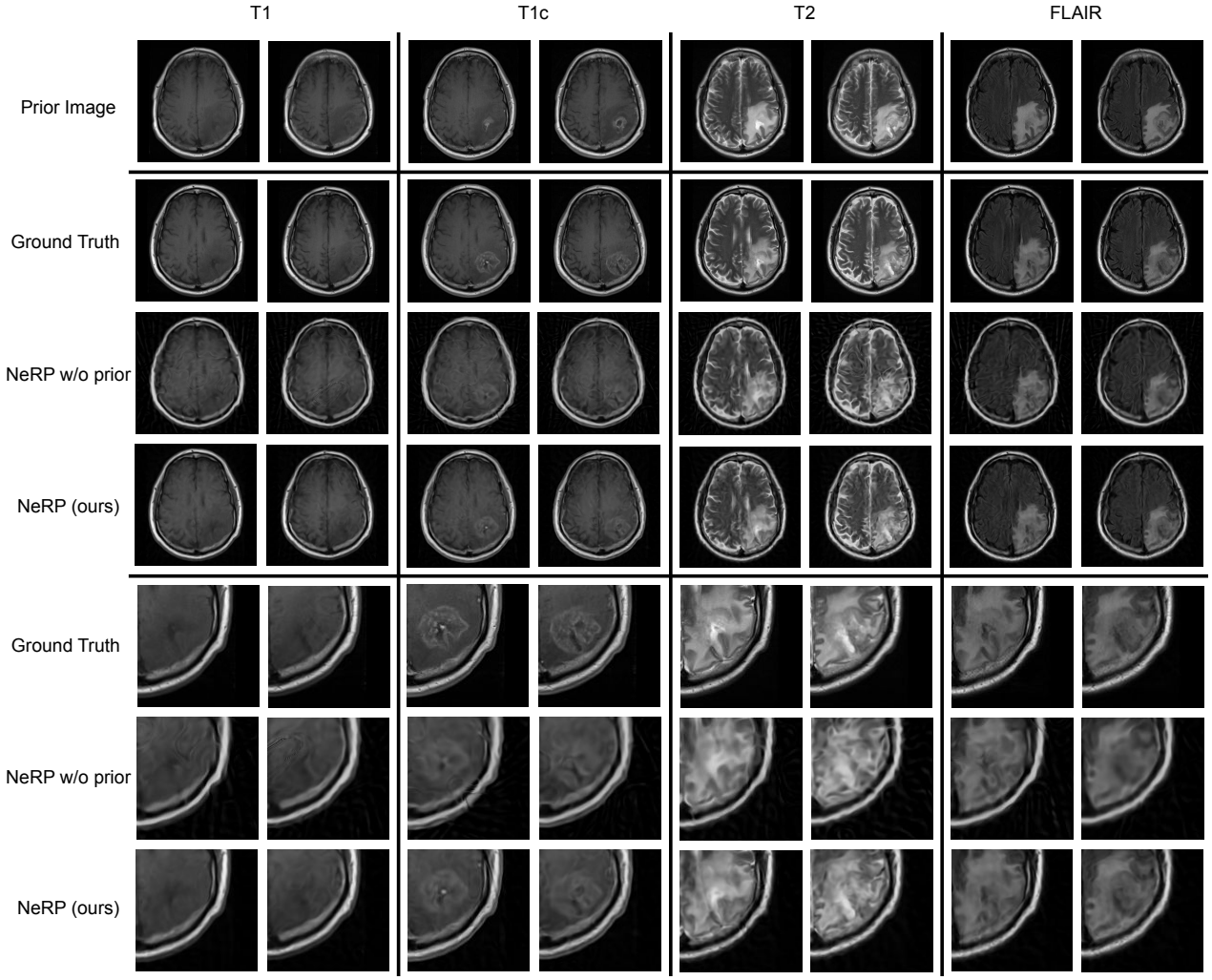

Fig. S1. Results of 2D MRI image reconstruction for multi-contrast MRI data using 40 radial spokes. The first and second rows show the 2D MRI images of the prior image (first exam) and the target image (second exam) for four image contrasts (T1, T1c, T2, FLAIR). The third and fourth rows show the reconstruction results by using the proposed NeRP method as well as the ablation study without using prior embedding. By zooming in the tumor regions, the last three rows show the cropped sub-images of the tumor regions corresponding to the images in the second, third, and fourth rows, respectively.